Dystrophin is a mechanical tension modulator

Arne D. Hofemeier[1,2*], *Till M. Muenker*[1], *Fabian Herkenrath*[1], *Mariam Ristau*[1], *Matthias Brandt*[1], *Mina Shahriyari*[2,3], *Malte Tiburcy*[2,3], *Wolfram H. Zimmermann*[2,3,4], *Christof Lenz*[5,6], *Kamel Mamchaoui*[7], *Anne Bigot*[7], *Penney M. Gilbert*[8,9,10], *Timo Betz*[1,4*]

[1]Third Institute of Physics, University of Göttingen, Germany

[2]Institute of Pharmacology and Toxicology, University Medical Center Göttingen, Germany

[3]DZHK (German Center for Cardiovascular Research), Partner site Göttingen, Germany

[4]Cluster of Excellence 'Multiscale Bioimaging: from Molecular Machines to Networks of Excitable Cells' (MBExC), University of Göttingen, Germany

[5]Department of Clinical Chemistry, University Medical Center Göttingen, Germany

[6]Bioanalytical Mass Spectrometry Group, MPI for Multidisciplinary Sciences, Göttingen, Germany

[7]Sorbonne Université, Inserm, Institut de Myologie, Centre de Recherche en Myologie, Paris, France

[8]Institute of Biomedical Engineering, University of Toronto, Canada

[9]Department of Cell and Systems Biology, University of Toronto, Canada

[10]Donnelly Centre, University of Toronto, Canada

[*]**Corresponding authors:** arne.hofemeier@phys.uni-goettingen.de, timo.betz@phys.uni-goettingen.de

Abstract

Duchenne muscular dystrophy (DMD) represents the most common inherited muscular disease, where increasing muscle weakness leads to loss of ambulation and premature death. DMD is caused by mutations in the dystrophin gene, and is known to reduce the contractile capacity of muscle tissue both *in vivo*, and also in reconstituted systems *in vitro*. However, these observations result from mechanical studies that focused on stimulated contractions of skeletal muscle tissues. Seemingly paradoxical, upon evaluating bioengineered skeletal muscles produced from DMD patient derived myoblasts we observe an increase in unstimulated contractile capacity that strongly correlates with decreased stimulated tissue strength, suggesting the involvement of dystrophin in regulating the baseline homeostatic tension level of tissues. This was further confirmed by comparing a DMD patient iPSC line directly to the gene-corrected isogenic control cell line. From this we speculate that the protecting function of dystrophin also supports cellular fitness via active participation in the mechanosensation to achieve and sustain an ideal level of tissue tension. Hence, this study provides fundamental novel insights into skeletal muscle biomechanics and into a new key mechanical aspect of DMD pathogenesis and potential targets for DMD drug development: increased homeostatic tissue tension.

Keywords: *Duchenne muscular dystrophy, bioengineered skeletal muscles, tensional homeostasis, contractile forces*

1 Introduction

Skeletal muscle is one of the most abundant tissues in the human body and its proper function is crucial for existential functions such as voluntary movement, thermogenesis, breathing and maintaining posture[43,27,10]. Dysregulation contributes to life-limiting genetic muscle disorders such as Duchenne muscular dystrophy (DMD), affecting 1 in 3500 - 5000 males live births[11], being the most common inherited muscular disease. Even though the causative gene *DMD* and its associated protein, dystrophin, is known and studied since the 1980s[25,13], DMD still is an incurable disease. Eventually this devastating disorder becomes lethal within the third decade of a patients' life due to cardio-respiratory failure[7].

Although affected boys appear clinically normal at birth, muscle biopsies reveal necrotic muscle fibers, tissue inflammation and fibrosis on a microscopic level even before the onset of typical symptoms[7,5]. Despite the commonality of a genetic dystrophin loss, an intriguing finding is that muscles decline in form and function at different paces when comparing distal and proximal muscle groups[15]. Characteristically, patients with DMD develop difficulties walking during childhood and later become wheelchair dependent in their teens[20]. As the disease progresses, DMD patients further lose upper body function leading to respiratory distress and cardiomyopathy[20,57]. Taken together, the pathological severity of DMD not only varies widely depending on the age of the patient but also on the muscle being evaluated[62,15].

In recent years, DMD research has led to the implementation of a variety of therapeutic approaches that indeed improve respiratory and motor function, e.g. corticosteroid anti-inflammatory drugs and exon skipping strategies. Unfortunately, these therapies only delay disease progression to a certain extent[36]. Gene therapy clinical trials are underway and offer a promising therapeutic approach[60]. However, the efficacy and long-term impact of such therapies in humans remains unknown. As such, more knowledge is urgently needed to fully understand the

development and progression of DMD from the molecular to the cellular and the system levels.

The protein impacted in DMD, dystrophin, is one of the largest intracellular proteins that links the actin cytoskeleton to the transmembrane dystroglycan protein complex. This triggered the hypothesis that it stabilizes the muscle cell membrane against forces by stretching like a spring during contraction[13]. The large number of spectrin repeats in the dystophin protein supports this idea as they can act as shock absorbers. Under high tension, folded spectrin repeats are known to unfold[48], thereby essentially relaxing the transmitted tension. Interestingly, the opening of spectrin repeats can also function as a mechanosensing mechanism by exposing cryptic binding sites. This was demonstrated in the case of α-actinin, another actin binding protein[53]. Besides these tension buffering, or even tension sensing capacities, dystrophin is proposed to be essential for force transmission between the acto-myosin contractile machinery and the sarcolemma, including its surrounding extracellular matrix (ECM)[3,18]. Loss of dystrophin leads to destabilization of the muscle fiber membranes which results in elevated intracellular calcium concentrations as well as reactive oxygen species (ROS) levels. Additionally, it is accompanied by the absence of neuronal nitric oxide synthase (nNOS) at the sarcolemma and reduced overall nitric oxide (NO) levels[9,23,4]. Although state of the art research can draw from multifactorial and complex experimental results, a coherent picture merging the many roles of dystrophin is still to be defined. Partially, this is due to missing genetic models that actualize the human DMD phenotype sufficiently. For instance, the sheer size of the dystrophin gene with 2.2 Mbp does not allow for simple replacement by mutants. Additionally, the most commonly used *mdx* mouse strain fails to recapitulate important phenotypic hallmarks observed in humans, such as the loss of ambulatory ability[61].

For this reason, numerous *in vitro* strategies have emerged in recent years for cultivating self-organizing, human multinucleated myotubes within 3D extracellular matrix (ECM) scaffolds[31,2,1,22]. Based on this, the first 3D bioengineered human

skeletal muscle disease models were reported only recently, and offer great opportunities to further fundamental research and drug development[32,44,42,17,55,51]. By contrast to 2D myotube culture, these approaches support studies of the force generating capacity of normal and DMD muscle tissue upon stimulating a contraction. However, in contrast to recent results showing that the constant tissue forces and tension are highly relevant in tissue development[14,21,1], studies on muscle functionality mainly focused on stimulated force generation, including DMD[17]. In doing so, a key parameter is less well studied; the homeostatic (e.g. baseline) tension of the tissue that is present even in the non-stimulated situation at rest and actively maintained. Therefore, the homeostatic tension is distinct from the commonly reported passive resting tension, which is affiliated to elastic forces in the connective tissue fraction of muscle and also to viscoelastic myofibrillar structures (e.g. titin) since decades[33,35,41]. As the resting tension is experimentally identified with the external load that allows the larges contractile force generation, the homeostatic tissue tension is furthermore a distinct quantity from a measurement point of view.

Even though tissues are known to actively regulate their tensional homeostasis[58] and the dystrophin binding partner nNOS was reported to play a crucial role in regulating mechanical loading in skeletal muscle[56,45,18] and relaxation of smooth muscles[19], the homeostatic tissue tension within skeletal muscle has not been in focus in the context of DMD, quite surprisingly.

In closing this knowledge gap, our study reveals a surprising, and initially counter-intuitive relationship, whereby strongly contracting healthy muscle tissues are antagonized by low homeostatic tension, while the DMD muscle tissues show a higher homeostatic tension but offer limited contractile function in response to electrical stimulation. This was further confirmed in a clean isogenic cell system where the presence of a truncated dystrophin protein in tissues showed increased homeostatic tension and decreased stimulated contraction when compared to tissues derived from the same cell line that had recovered a functional dystrophin

protein by CRISPR/Cas9 mediated exon skipping, supporting its central role in mechanosensation.

2 Results and Discussion

2.1 Myotube and muscle tissue morphology is dependent on dystrophin

Skeletal muscle precursor cells, also called 'myoblasts', can be isolated from patients' biopsies and immortalized for further long-term applications[34]. Here, we used cell lines derived from 6 different donors and from biopsies originating from three different muscle groups (Table 1). As recently reported, all of these cell lines are capable of forming functional biomimetic skeletal muscle tissues within 3D protein scaffolds by self-organizing around two vertical posts[42,17]. With these human immortalized myoblast cell lines from healthy and DMD backgrounds, and our previously developed glass bottom chamber for high resolution imaging[22], we cultured bioengineered skeletal muscles within a 3D fibrin-Geltrex™ scaffold over two weeks (Figure 1 a-d). All of the human immortalized cell lines self-organized nicely to form tissues around the two posts (Figure 1 e). Precise measurement of the tissue width revealed that dystrophic tissues are on average thinner when compared to healthy tissues (Figure 1 g). The resulting averages are dominated by drastically reduced dystrophic tissue widths of bioengineered skeletal muscles derived from cells that originated from leg muscle biopsies (Figure 1 h). By contrast, bioengineered dystrophic skeletal muscle tissues produced using cells originating from paravertebral biopsies are slightly thicker. Additionally, when investigating the myotubes formed within the bioengineered skeletal muscles at two weeks of differentiation, more morphological differences become apparent between the healthy and dystrophic tissues (Figure 1 f). Although immunohistological staining revealed multinucleated myotube formation in all models, in general the dystrophic tissues using cells derived from leg muscle biopsies exhibit immature and thinner myotubes that lack sarcomere structures aligning in parallel.

Overall, the dystrophic myotubes were smaller in width (Figure 1 i). One exceptional case was myotubes within tissues produced using the paravertebral derived DMD5 cell line, where only insignificant differences were observed (Figure 1 j). DMD5 has an exon 2 duplication which is susceptible to revertant fiber formation due to an alternative translation initiation site in exon 6[59], a phenotype we observe in tissues produced using this line (Supplement 1). These data are in exact compliance with previous reports of Ebrahimi et al.[17], who very recently found revertant fiber formation in DMD5 bioengineered muscles for the first time. In sum, these results suggest that the cell line biopsy tissue origin can be reflected by phenotypes observed *in vitro* in bioengineered tissues, and are consistent with clinical results concluding that different muscle groups are affected by DMD with different severity[15].

2.2 Stimulated contractility versus homeostatic tissue tension

Since the human dystrophic skeletal muscle tissues showed gross morphological differences when compared against healthy tissues, we next investigated their functional contractility. Here, we sought to distinguish between the two types of contractile forces that the bioengineered muscles exert on the posts. First, the stimulated contractility that is widely used to examine muscle strength upon a stimulus, e.g. electrical pulses. Second, the unstimulated contractile force of the bioengineered tissue that to this point has not been in the focus of the field, and which we term the 'homeostatic tissue tension'. Homeostatic tissue tension is the post deflection that naturally arises during tissue development, and is mediated by active contractile forces cells exert on their environment. We therefore distinguish the homeostatic tension from the passive resting tension that is related to connective tissue stiffness and elastic myofibrillar proteins[33,35,41].

To study the stimulated tissue contractility, we positioned electrodes exactly behind each vertical post and electrically stimulated the bioengineered skeletal muscle tissues with a pulsed electrical field of 5 V at 20 Hz to investigate full tetanus

2.2 *Stimulated contractility versus homeostatic tissue tension*

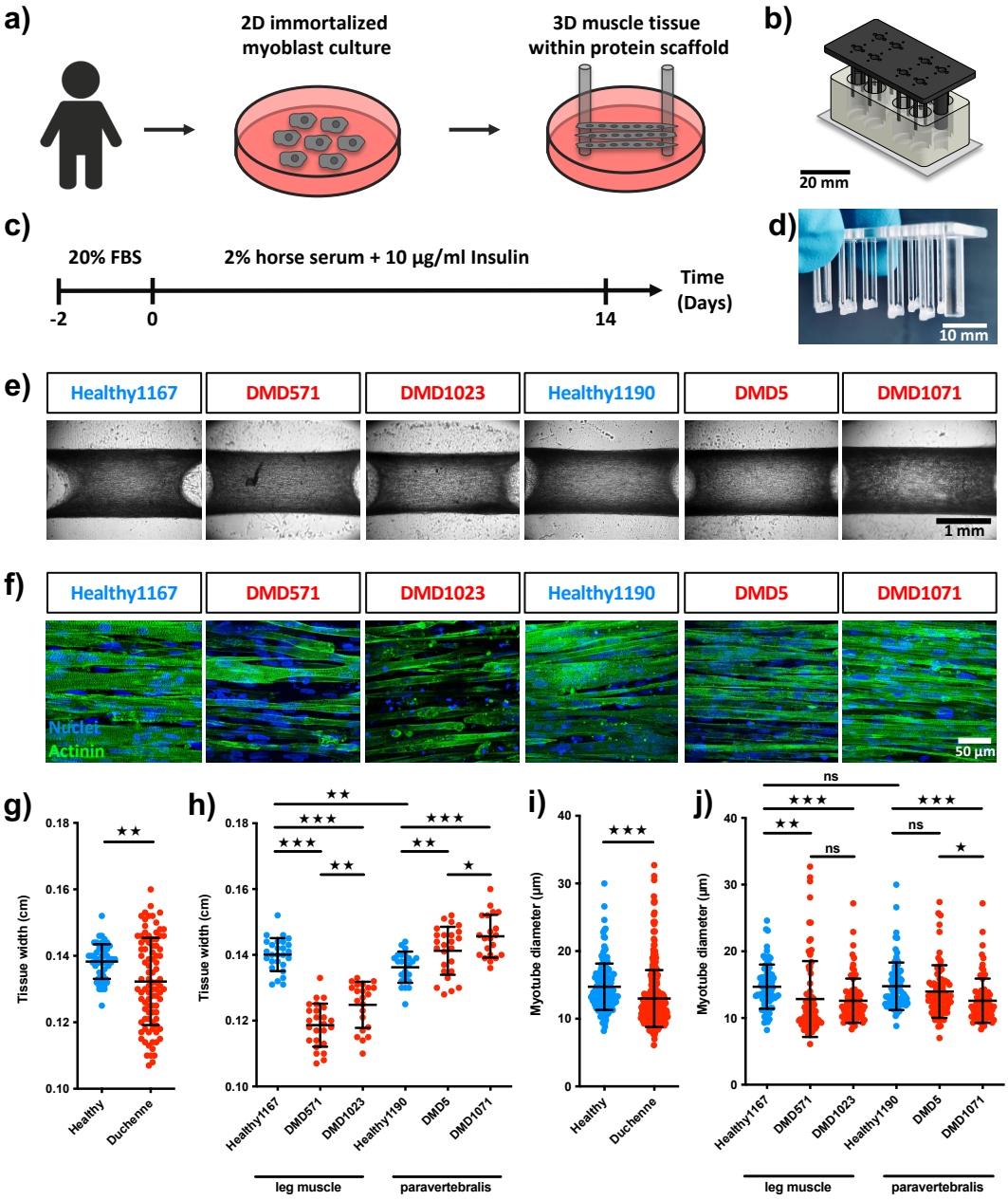

Figure 1: Tissue appearance and myotube diameter size evaluation of bioengineered dystrophic human skeletal muscles. a) Schematic overview of 3D bioengineered skeletal muscle tissue generation within our PMMA culture mold (b). c) Timeline of 3D human skeletal muscle tissue cultivation *in vitro*. d) Representative capture of two weeks old human bioengineered skeletal muscle tissues anchored to the tips of the PMMA posts. e) Representative brightfield images of two weeks old healthy and DMD human skeletal muscle tissue *in vitro*. f) Representative flattened confocal stacks of multinucleated myotubes within healthy and DMD human skeletal muscle tissue immunostained for sarcomeric-alpha-actinin (green) and nuclei counterstained with DRAQ7 (blue). g-h) Tissue width of healthy and DMD human skeletal muscle tissue, pooled (g) and separated between the different patients (h). i-j) Myotube diameter of healthy and DMD human skeletal muscle tissue, pooled (i) and separated between the different patients (j).

strength (Figure 2 a, Supplement 2). Since these electrodes tightly fit into the holes present on the lid of the chambers, we can assure a very similar position in every experiment. During stimulated contraction, healthy as well as dystrophic skeletal muscle tissues exerted sufficient forces to deflect the posts (Figure 2 b, Supplement 3). Using the spring constant of the posts reported in our previous studies[22], we calculated the contractile forces of healthy and dystrophic skeletal muscle tissues upon electrical stimulation. As expected, healthy bioengineered skeletal muscle tissues typically exerted more force on the posts ($\sim 0.2 \pm 0.1$ mN) during a 20 Hz stimulated tetanus contraction when compared to tissues from a dystrophic background, which exerted around 0.1 ± 0.1 mN in average (Figure 2 c). When comparing the different donor-derived skeletal muscle tissues separately, we found that this phenotype was more pronounced in the tissues produced using myoblasts from a leg muscle group background (Figure 2 d). The Healthy1167 cell line elicited almost 0.2 ± 0.1 mN stimulated contractile force. However, DMD571 and AB1023 did not even reach 0.05 ± 0.02 mN on average. Again, the paravertebral derived DMD5 cell line breaks ranks with a stimulated contractile force of more than 0.2 ± 0.09 mN on average that is similar to the paired healthy sample. Paravertebral derived DMD1071 was significantly weaker than the paravertebral derived Healthy1190. Taken together, these data are consistent with previous reports[17], which stresses the reliability of our system. Interestingly, the stimulated contractile forces of the human immortalized myoblast derived tissues strongly correlated with the myotube diameter (Supplement 4). This observation may support functional estimations of the biomimetic skeletal muscle tissues strength from morphological data in the future.

Against intuition, we observed an inverse relationship between the level of stimulated contractility and the measured homeostatic tissue tension. Specifically, dystrophic bioengineered muscle tissues showed an overall higher homeostatic tissue tension (1.2 ± 0.6 mN) compared to the healthy controls (0.7 ± 0.4 mN) (Figure 2 e). Again, this phenotype is dominated by the significant differences observed

from cell lines derived from leg muscle biopsies (Figure 2 f) wherein the homeostatic tissue tension was increased two to threefold in DMD compared with the healthy bioengineered muscles. Indeed, the homeostatic tissue tension is the dominant force exerted on the vertical post as it is more than three times higher on average than the stimulated tetanus contraction of healthy bioengineered muscle tissues. For dystrophic bioengineered muscles, the homeostatic tissue tension was more than ten times higher than the stimulated contractile force emphasizing the severe imbalance of these two mechanical properties.

Next we wondered if there was a correlation between the stimulated and homeostatic force generation. To test this, we normalized the stimulated and homeostatic forces to the healthy tissue controls and analyzed them in a scatter plot. This analysis revealed a strong anticorrelation between homeostatic tissue tension and the contractile force generation (Figure 2 g). In simple words, the reduced stimulated contractility of diseased muscles is accompanied by a relative increase in homeostatic tension. This suggests an interesting new hypothesis, namely that the poor stimulated contractility of DMD derived bioengineered muscles is due to the elevated homeostatic tissue tension that leads to an incapability of the tensed tissues to contract further. To extend this point, it is as if the diseased muscle is wasting a large fraction of finite force generation capacity in the unstimulated situation.

This novel DMD biomechanical finding is in compliance with common clinical reports of stiffened Duchenne skeletal muscles[26], which was concluded to be the effect of progressing fibrosis. Since the myoblast cell lines are clonally derived[34], without any fibroblasts or other cell types, we speculate that increased homeostatic tissue tension in dystrophic skeletal muscles may additionally contribute to higher muscle stiffness. Intrigued by these new insights, we wondered if the elevated homeostatic tissue tension in dystrophic bioengineered skeletal muscles is a tissue phenomenon or the outcome of already mechanically ill-equipped single cells.

2.2 *Stimulated contractility versus homeostatic tissue tension*

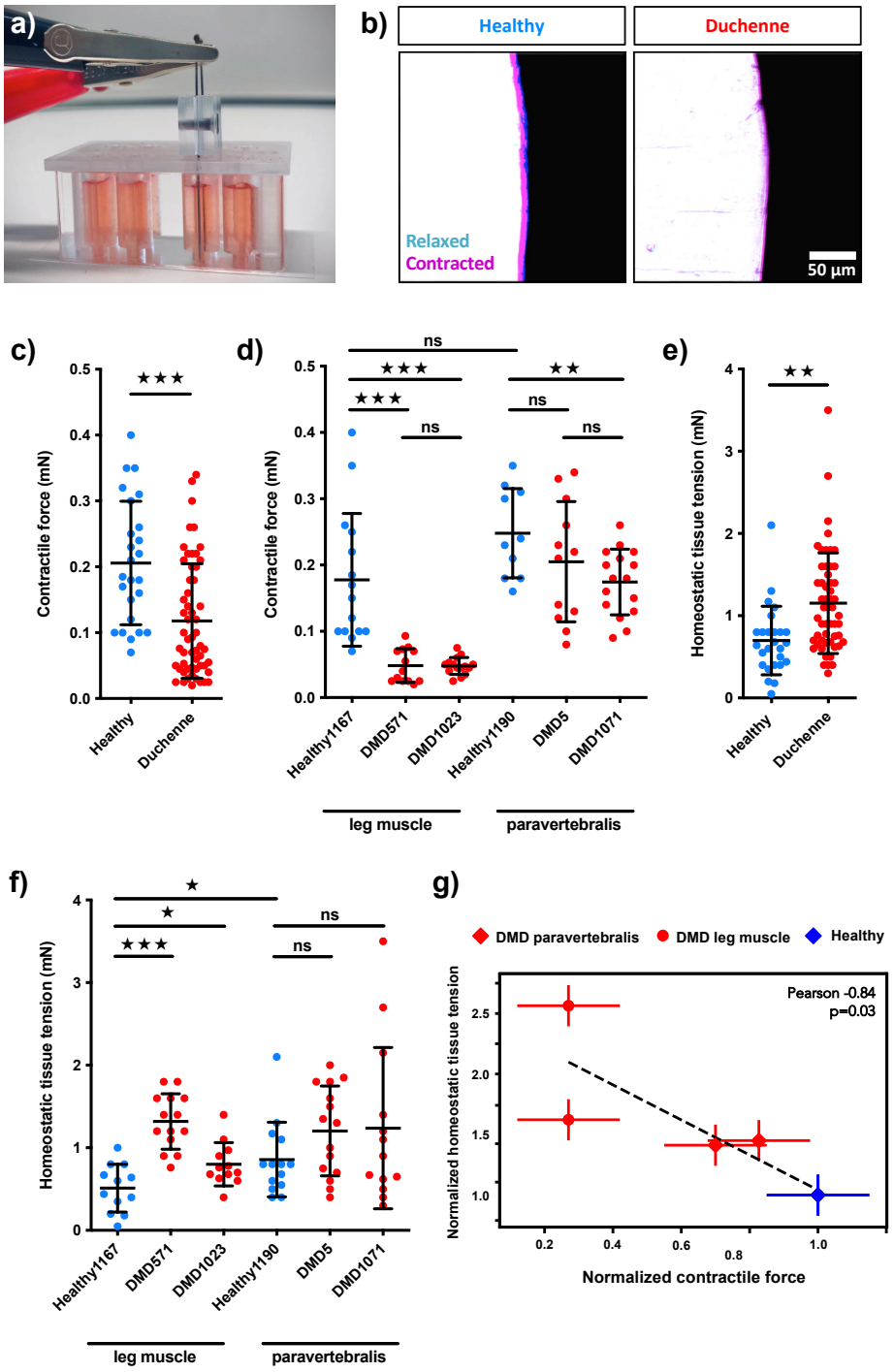

Figure 2: Quantification of human dystrophic skeletal muscles' contractile forces and homeostatic tissue tension. a) Setup for electrical stimulation of human skeletal muscle tissues *in vitro*. b) Post deflection by healthy and DMD human bioengineered skeletal muscle tissues within PMMA culture mold upon 20 Hz electrical stimulation. c-d) Contractile force of healthy and DMD human skeletal muscle tissues upon 20 Hz electrical stimulation, pooled (c) and separated between the different patients (d). e-f) Homeostatic tissue tension of healthy and DMD human bioengineered skeletal muscle tissues, pooled (e) and separated between the different patients (f). g) Anti-correlation between the normalized contractile force and homeostatic tissue tension of healthy and DMD bioengineered muscles.

2.3 TFM reveals increased contractile moment of DMD myoblasts

To compare the homeostatic force generation properties at the tissue level to those as the single myoblast level, we exploit the fact that they both mechanically interact and pull on their environment, which can be quantified by the contractile moment determined by Traction Force Microscopy (TFM)[12,29,47,8]. Therefore, we performed TFM of single myoblasts on physiological 15 kPa (Young's modulus) PAA gels that include fluorescent nanoparticles to track potential deformations (Figure 3 a). By analysing the bead displacements within the PAA substrate, we obtained force maps of the single myoblasts pulling on the PAA gels (Figure 3 b). Comparing the human immortalized myoblasts from healthy and DMD patients, we found that, on average, single DMD myoblasts pulled more strongly on their culture substrates than did the healthy cells (Figure 3 c). This phenomenon is again most significant in myoblasts derived from leg muscle biopsies (Figure 3 d). Hence, the single myoblast contractility confirms the altered homeostatic tissue tension of dystrophic bioengineered muscles.

To better further characterize the extent to which the 3D homeostatic tension of bioengineered muscle tissue can be explained by the single cell contractile moment, we looked at the overall correlation between these two quantities. As expected from the already found results, the contractile moment of the myoblasts strongly correlates with the homeostatic tension on a tissue level (Figure 3 e). This suggests that the elevated dystrophic tissue tension is not a collective tissue effect but can be explained, at least in part, by an increased contractility on the single myoblast level. This interpretation reinforces, that the homeostatic tension of a tissue is, in contrast to the passive resting tension, actively regulated by the cell since undifferentiated DMD myoblasts are indeed mechanically ill-equipped. Further, these results underscore a new influence of dystrophin in healthy myoblasts, even though we and others[16] find it is expressed at low levels (Figure 3 f). To our knowledge, DMD myoblast traction forces have not been studied, yet, which

underlines the potential of the new insights by quantifying the tensional homeostasis in the context of skeletal muscle diseases. Very recently, pathological DMD-related dystrophin mutations were reported to lead to lower focal adhesion tension in a FRET-based C2C12 model[46]. Although this may sound contradictory to our results, it can be explained by larger focal adhesion sites, effectively distributing the increased forces over more molecules. In any case, this stresses the complexity of the emerging dystrophin-associated mechano-signaling and highlights the independence across single focal adhesion and whole cell mechanical length scales.

2.4 Biomimetic DMD model exhibits pathological disease features

Throughout our whole study we found phenotypical variability and a large spread across our patient-derived data. Consistently, for myotube diameter (Figure 1 j), stimulated tissue contractility (Figure 2 d), homeostatic tissue tension (Figure 2 f) and single myoblast traction forces (Figure 3 d), we observe the most pronounced DMD phenotype when comparing leg muscle derived cell lines. By contrast, paravertebral derived single myoblasts and bioengineered muscles did not exhibit expected DMD phenotypes to a similar extent. Whereas this may sound like a poor DMD model on the first glance, it in fact reveals the great sensitivity of it. Disease severity can depend on the muscle group being evaluated and DMD as disease progresses symptomatically from distal (e.g. quadriceps) to proximal (e.g. paravertebral muscles) muscle groups[20,62,15]. This may explain why we saw a more pronounced functional disability and deregulation of the mechanical homeostasis in leg derived bioengineered muscles throughout all of our experiments. To this end, our DMD model displays typical pathological features of the disease. In addition, the paravertebral muscles originate from an epaxial background, which are embryologically distinct from the hypaxial myotome (e.g. quadriceps) and may provide another reason for differences within our bioengineered muscles[54]. Concluding, the muscular origin of cell isolation seems to play a crucial role for bioengineering DMD models in the future. Since the immortalized patient-derived

2.4 Biomimetic DMD model exhibits pathological disease features

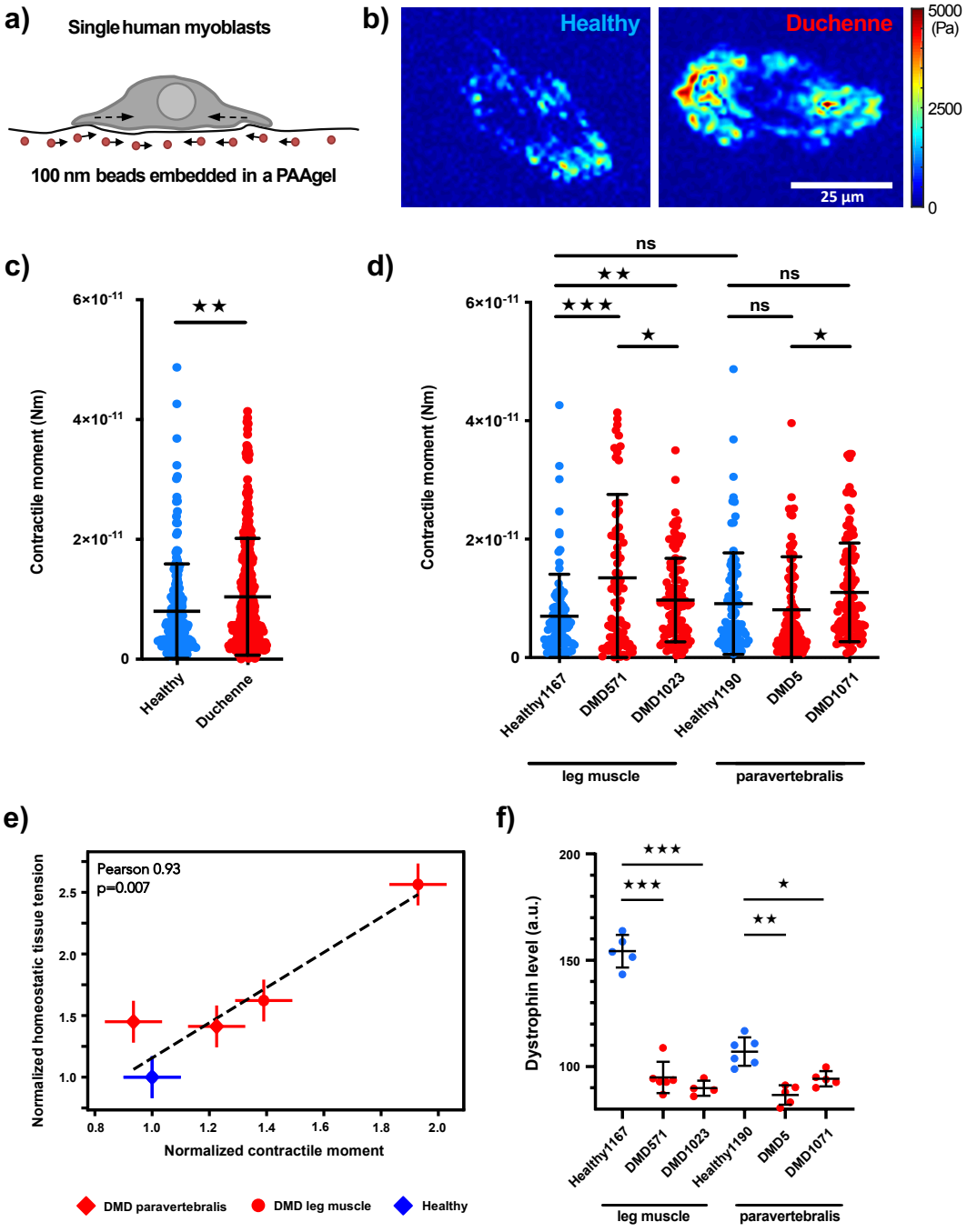

Figure 3: Homeostatic contractility of single DMD myoblasts. a) Schematic sketch of a single myoblast on a PAA gel for traction force microscopy (TFM). b) Representative force map of a healthy and DMD myoblast obtained through TFM. c-d) Contractile moment of healthy and DMD single myoblasts, pooled (c) and separated between the different patients (d). e) Correlation between the normalized contractile moment of single myoblasts and homeostatic tissue tension of healthy and DMD bioengineered muscles. f) Changes in dystrophin levels of healthy and DMD myoblasts determined by data independent acquisition mass spectrometry (DIA-MS).

myoblasts originate from isolated muscle stem cells (MuSCs), we can speculate, that the MuSC population in dystrophic epaxial paravertebral muscles may not be as exhausted as in leg muscles.

2.5 Increased DMD homeostatic tissue tension is confirmed by an isogenic model

In biomimetic skeletal muscles raised from patient-derived immortalized myoblasts we observed an overall higher homeostatic tissue tension in our DMD model that strongly correlates with a decreased stimulated contractility (Figure 2 g). However, patient-derived cells exhibit immense phenotypical variability. Hence, we sought to demonstrate the close connection of the homeostatic tissue tension and functional strength to the dystrophin protein in an isogenic culture system. For this reason, we investigated an established iPSC line using cells from a Duchenne patient with an exon 48-50 deletion ('DMD51') in the dystrophin gene and compared it to the 'Cor51' iPSC line that was genetically corrected via exon 51 skipping (Figure 4 a)[30]. The isogenic cell lines were differentiated into skeletal myocytes as previously described[51] and used to bioengineer skeletal muscles in our glass bottom chamber over a period of 4 weeks.

We would expect that the tensional homeostasis is disturbed in DMD51 muscles, and restored in Cor51. Morphologically, we found that Cor51 showed multinucleated, striated myotubes in a more dense assembly when compared to DMD51 tissues (Figure 4 b). In addition, the myotubes formed from the Cor51 cells were also significantly thicker (Figure 4 d), which is in compliance with an overall higher macroscopic tissue width of the Cor51 engineered skeletal muscles (Figure 4 c). These dystrophin-dependent effects in the isogenic cell model are comparable to those we observed in patient derived pooled muscle tissues (Figure 1 g, i). Hence, this already hints towards an elevated homeostatic tissue tension and a lower stimulated contractile strength of DMD51 bioengineered skeletal muscles when compared to the genetically corrected Cor51 tissues. As expected, the peak

force of Cor51 engineered skeletal muscles was significantly higher following a 20 Hz electrical stimulation when compared to stimulated DMD51 tissues (Figure 4 e), supporting prior results on bioengineered heart muscle tissue showing that this dystrophin correction improves stimulated 3D engineered heart muscle tissue contraction[30]. Furthermore, we again find a significant increase in homeostatic tension in the DMD51 tissue, when compared to the Cor51 tissue (Figure 4 f). This directly confirms our results in tensed dystrophic skeletal muscle tissues raised from patient-derived immortalized myoblasts.

Therefore, these results demonstrate that dystrophin, besides its shock absorbing function, plays a central role in the modulation of homeostatic tissue tension, and that this new, quantitative parameter should be included in any study of muscle function and malfunction. The increased homeostatic tension may also explain partially the higher cell death and membrane ruptures found in DMD muscles, as the cells are continuously operating at a much larger force generation, which might increase the probability of fiber damage. Indeed, these findings suggest a novel role for dystrophin as a tension sensor and regulator to establish an intact tensional homeostasis (Figure 4 g).

2.6 Dystrophin as a potential tension sensor

Myoblasts and biomimetic skeletal muscle tissues from a hypaxial dystrophic background exhibited elevated traction forces (Figure 3 d) and homeostatic tissue tension (Figure 2 f, Figure 4 f). Therefore, lack of a dystrophin protein displays a dysregulated tensional homeostasis in these cells, which suggests a tension sensor and regulator function for dystrophin (Figure 4 g). The high number of spectrin repeats that are known to unfold under critical pulling forces[48] suggests a direct mechanistic role of these, similar to the mechanosensing reported by the unfolding of similar spectrin repeats in α-actinin[53]. The tension-dependent unfolding and refolding capability of these spectrin-like repeats was recently demonstrated experimentally, and was interpreted as a shock absorbing function of dystrophin[28].

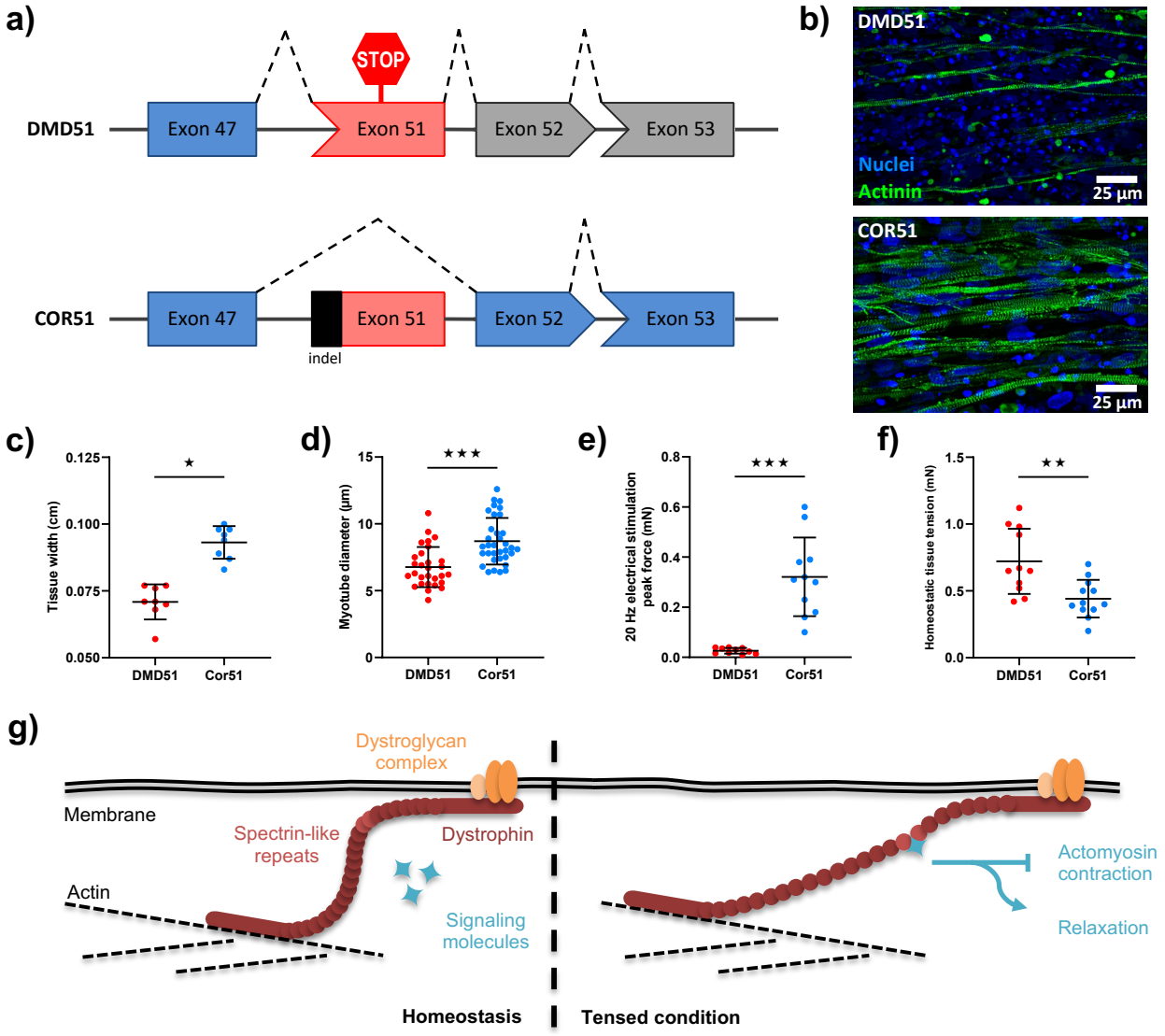

Figure 4: Exon 51 skipping in DMD51 restores tissue strength and tensional homeostasis. a) Schematic sketch of exon 51 skipping approach in iPSCs of DMD patients with exon 48-50 deletions. b) Representative flattened confocal stacks of multinucleated myotubes within DMD51 and Cor51 biomimetic muscles immunostained for sarcomeric-alpha-actinin (green) and nuclei counterstained with DRAQ7 (blue). c) Tissue width of DMD51 and Cor51 human biomimetic skeletal muscles. d) Myotube diameter of DMD51 and Cor51 human biomimetic skeletal muscles. e) Contractile force of DMD51 and Cor51 human biomimetic skeletal muscles upon 20 Hz electrical stimulation. f) Homeostatic tension of DMD51 and Cor51 human biomimetic skeletal muscles. g) Hypothetical model of Dystrophin acting as a tension sensor that regulates the cells' tensional homeostasis.

However, this exact mechanism may additionally reveal binding sites upon tension for downstream signaling proteins (Figure 4 g). To explain the observed down-regulation of homeostatic tension in the presence of dystrophin, a molecule that is known to relax muscle contraction would be required to bind to a cryptic binding site that is only revealed if the tension surpasses a critical value. Indeed, dystrophin is known to interact with proteins that regulate mechanical loading in skeletal muscles and relaxation in smooth muscle (e.g. nNOS)[19,56,45,18]. Hence, in line with this tension sensor model, it is not surprising that dystrophic cell lines show deregulated, and more specifically, elevated homeostatic tension. Our measurements support the hypothesis that dystrophin acts as a tension sensor where mechanical signaling proteins, like nNOS, may bind to dystrophin in a stretched or tensed condition and thus maintain the proper tensional homeostasis of healthy skeletal muscle (Figure 4 g).

This new model provides a simple explanation for the surprising increase of homeostatic tension in dystrophic muscle, despite possessing reduced stimulated contractility when compared to healthy muscle. We suggest that a lack of dystrophin impairs intracellular sensing of critically high stresses. This deregulation may lead to an increased homeostatic tension which could result in elevated cellular damage. Assuming a limited force generation capacity of a muscle fiber, less contraction can be applied if the steady state, hence homeostatic, force generation is already elevated. This model is directly supported by the observed anticorrelation between homeostatic tension and stimulated force generation.

3 Conclusion

Here, we reported a novel mechanical key feature of Duchenne muscular dystrophy: Elevated homeostatic tissue tension (Figure 2 e, Figure 4 f). Our data suggest that tensional homeostasis within skeletal muscle tissue is crucial for proper functionality (Figure 2 g) since increased homeostatic tissue tension strongly correlated with decreased contractile strength upon stimulation. Furthermore, if the homeostatic, hence constant tension exceeds a maximal bearable level, this can furthermore explain the increased cell death as found in dystrophic muscles. Our results shine light on potential new fundamental functions of the dystrophin protein as a potential tension sensor protein (Figure 4 g) in addition to its proposed stabilizing function[28]. In addition, our findings stress the importance of a highly regulated tensional homeostasis in skeletal muscle cells since we found that single dystrophic myoblasts show an overall increase in contractile moment (Figure 3 c). In the future, this may provide new therapeutic targets aimed at interfering with muscle contractility/relaxation signaling to reduce characteristic progressive DMD muscle injuries and MuSC pool exhaustion as a strategy to prolong the life span of patients. Especially, a precise inhibition of homeostatic tension could be predicted as possible treatment beyond the current developed therapies.

4 Experimental Section

PMMA chamber fabrication for 3D muscle tissue culture:
Muscle tissue culture molds were fabricated from polymethyl methacrylate (PMMA) and glued onto a microscopy cover glass (VWR, Radnor, USA) as previously described[22]. Prior to use, the molds were sterilized using 70 % ethanol and the wells were coated with a Poloxamere solution in ddH_2O over night at 4 °C (5 % Pluronic® F-127, Sigma, St. Louis, USA) to render the surface non-adhesive.

Human immortalized myoblast line cultivation:

All immortalized human muscle progenitor cell lines (Table 1) were established at the Myoline platform of the Institut de Myologie (Paris, France)[34]. The cells were cultivated in tissue culture flasks (75 cm^2, Greiner) in a Skeletal Muscle Cell Growth medium kit (PROMOCELL) supplemented with 15 % fetal calf serum (FCS, Sigma) and 1 % penicillin-streptomycin (Gibco) at 37 °C and 5 % CO_2 in a humidified incubator. Skeletal Muscle Cell Growth medium was changed every other day. At 80 % confluency the cells were split using 0.25 % Trypsin-EDTA solution (Sigma).

cell line name	**phenotype**	**mutation in DMD**	**origin**	**age**
Healthy1167	healthy	none	fascia-lata	20
Healthy1190	healthy	none	paravertebral	16
DMD571	Duchenne	Deletion exon 52	fascia-lata	10
DMD1023	Duchenne	Stopp codon exon 59	quadriceps	11
DMD5	Duchenne	Duplication exon 2	paravertebral	14
DMD1071	Duchenne	Deletion exon 45-52	paravertebral	13

Table 1: Human immortalized patient derived myoblasts used in this study.

Myogenic differentiation of iPSCs:

Human induced pluripotent stem cell (iPSC) line DMD Del48-50 (DMD51) was purchased from RIKEN BioResource Center (HPS0164). The genetic correction of DMD51 by CRISPR/Cas9 mediated gene editing (Cor51) has been described before[30]. DMD51 and isogenic Cor51 lines were maintained on Matrigel-coated flasks in StemMACS iPSC Brew medium. Directed differentiation into skeletal myocytes was performed as previously reported by Shahriyari et al. 2022[51]. In brief, iPSC were seeded in iPS-Brew XF medium with 5 µmol/L of Y27632 (Stemgent) for 24 hrs to obtain a 30 % confluent culture. To start differentiation, medium was switched to DMEM (Thermo Fisher Scientific) with 1 % Pen/Strep, 1 % N-2 Supplement, 1 % MEM non-essential amino acid solution (N2 basal medium, all Thermo Fisher Scientific), 10 µmol/L CHIR99021 (Stemgent), 0.5 µmol/L LDN193189 (Stemgent), and 10 ng/ml FGF-2 (Peprotech) for 4 days. At

day 4, the medium was exchanged with N2 basal medium, 20 ng/ml FGF-2, and 10 µmol/L DAPT (Tocris) until day 6. On day 6 and 7, 10 ng/ml HGF (Peprotech) was added to the medium. The medium was then switched to N2 basal medium, 10 µmol/L DAPT, 10 ng/ml HGF, and 10 % knockout serum replacement (Thermo Fisher Scientific) on days 8, 9, 10 and 11. From day 13 to 22, myogenic cells were expanded in N2 basal medium, 10 % knockout serum replacement, and 10 ng/ml HGF. Day 22 skeletal myocytes were then enzymatically dissociated with TrypLE (Thermo Fisher Scientific) for 5 to 7 minutes at 37 °C and frozen in expansion medium with 5 µmol/L Y27632 (Stemgent).

3D human skeletal muscle microtissue cultivation:

3D skeletal muscle tissues were raised in culture as previously reported by various groups[31,2,22]. Briefly, 1.5 x 10^7 cells per ml were resuspended in an ECM mixture consisting of DMEM (40 % v/v, Capricorn, Ebsdorfergrund, Germany), 4 mg/ml bovine fibrinogen (Sigma) in 0.9 % (w/v) NaCl solution in water and Geltrex™ (20 % v/v, Gibco). 25 µl of the cell mixture was used to seed each tissue. Fibrin polymerisation was induced with 0.5 units thrombin (Sigma) per mg of fibrinogen for 5 min at 37°C. Subsequently, 400 µl Skeletal Muscle Cell Growth medium supplemented with 1.5 mg/ml 6-aminocaproic acid (ACA, Sigma) was added. After 2 days, the growth medium was exchanged to differentiation medium containing DMEM supplemented with 2 % horse serum (HS, Sigma), 1 % penicillin-streptomycin (Gibco), 2 mg/ml ACA and 10 µg/ml human recombinant insulin (SAFC Biosciences). The differentiation medium was changed every other day. DMD51 and Cor51 derived bioengineered skeletal muscles were reconstituted in expansion medium (N2 basal medium, 10 % knockout serum replacement, and 10 ng/ml HGF) for one week followed by maturation in DMEM with 1 % Pen/Strep, 1 % N-2 Supplement, and 2 % B-27 Supplement (maturation medium) for additional three weeks.

Immunostaining and confocal fluorescence microscopy:

Confocal microscopy and immunohistological investigations were performed as previously reported[22]. In brief, human 3D skeletal muscle tissues were fixed using 4 % paraformaldehyde (PFA) for 15 min at room temperature within the culture mold. Next, the samples were blocked for 1 h at room temperature using PBS supplemented with 20 % goat serum (GS, Sigma) and 0.2 % Triton-X-100 (Carl Roth). Afterwards, the tissues were incubated with the primary antibody (monoclonal mouse anti-sarcomeric alpha actinin, 1:100, Abcam; monoclonal mouse anti-Dystrophin, 1:100, Santa Cruz Biotechnology) diluted in blocking solution over night at 4 °C. Subsequently, the tissues were washed with blocking solution three times and incubated with the respective secondary antibody (polyclonal goat anti-mouse IgG1, 1:500, Invitrogen) for 45 min at room temperature. Cell nuclei were counterstained using DRAQ7 (1:100, Abcam). Confocal images were acquired using Slidebook 6 software (3i) using an inverted microscope (Nikon Eclipse Ti-E) equipped with a CSU-W1 spinning disk head (Yokogawa) and a scientific CMOS camera (Prime BSI, Photometrics). Images were analysed and prepared for publication using the open source software Fiji[49].

Electrical stimulation of biomimetic human skeletal muscle tissues:

Contractile function of human 3D skeletal muscle tissues was examined two weeks after differentiation of immortalized myoblasts or four weeks after iPSC-derived tissue maturation. For that purpose, a metal pin (0.55 mm in diameter, Fine Science Tools) was implanted behind each post as electrodes. Via copper wires the electrodes were directly connected to a multi-function input/output unit (National Instruments) accessed by a custom written program[38]. The tissues were stimulated using square-wave pulses with 20 % duty cycle, 5 V amplitude and 20 Hz frequency (tetanus contraction). Time lapse videos of the posts during contraction were subsequently used for post deflection analysis.

Homeostatic tension analysis of biomimetic human skeletal muscle tissues:
The homeostatic tension of human 3D skeletal muscle tissues was evaluated two weeks after differentiation of immortalized myoblasts or four weeks after iPSC-derived tissue maturation. For that purpose, the distance of the two posts was measured directly after the seeding procedure and after tissue maturation. The reduction in post distance was multiplied by the posts' spring constant (39 µN/µm,[22]) to obtain the homeostatic tissue tension. The distances of the posts was measured using an custom written program[40]. In the rare event of a negative tension outcome the measurement was discarded.

Post deflection analysis:
For post deflection analysis, we proceeded as previously described[22]. In brief, we focused on the edge of the post with our imaging system while tissue contraction and recorded a time series. Following the deflection of the post throughout the whole time series with a custom written program[39], the pulling forces were determined by multiplication of the post displacement by the apparent spring constant of the post.

Traction force microscopy (TFM):
In this study, the traction forces of healthy and DMD single human myoblasts on 15 kPa (Young's Modulus) polyacrylamide (PAA) gels with 100 nm polystyrene beads (1:50, micromod) embedded were examined as previously described[50]. Briefly, TFM was performed 12-18 hours after seeding 1 x 10^5 cells on the fibronectin (Sigma) coated PAA gel surface within a 35 mm glass bottom dish (Greiner). Utilizing a 40X WI objective two z-stack images were acquired, one showing the cells on the substrate, the second image after cell lysis induced by addition of 500 µl of 5 % SDS. The bead displacement between the two images was used to calculate forces and deformation energies using Elastix software[24,52] embedded in a custom-made MATLAB (MathWorks) script[8]. In a next step, the background variances were reduced using Tikhonov's regularization and Bayesian theory. The

evaluation of traction forces and the resulting contractile moments were restricted to the cell-area set by previously defined masks which cover the cell area.

Mass spectrometry sample preparation:
Protein samples were prepared by lysis of 5 x 10 cells/ml for 5 min at 95 °C in SDS sample buffer composed of 62.5 mM Tris/HCl (pH 6.8), 10 % glycerol, 2 % sodium dodecyl sulfate, 5 % beta-mercapto-ethanol and 0.005 % bromphenol blue. The samples were loaded onto a 4-12 % NuPAGE Novex Bis-Tris Minigels (Invitrogen) and run into the gel for 1.5 cm. Following Coomassie staining, the protein areas were cut out, diced and subjected to reduction with dithiothreitol, alkylation with iodoacetamide and finally overnight digestion with trypsin. Tryptic peptides were extracted from the gel, the solution dried in a Speedvac and kept at -20°C for further analysis[6]. Protein digests were analyzed on a nanoflow chromatography system (nanoElute) hyphenated to a hybrid timed ion mobility-quadrupole-time of flight mass spectrometer (timsTOF Pro, all Bruker). In brief, 400 ng equivalents of peptides were dissolved in loading buffer (2 % acetonitrile, 0.1 % trifluoroacetic acid in water), enriched on a reversed-phase C18 trapping column (0.3 cm × 300 µm, Thermo Fisher Scientific) and separated on a reversed-phase C18 column with an integrated CaptiveSpray Emitter (Aurora 25 cm × 75 µm, IonOpticks) using a 100 min linear gradient of 5-35 % acetonitrile / 0.1 % formic acid (v:v) at 250 nl min^{-1}, and a column temperature of 50C. Both identification and quantification was achieve by directDIA analysis in diaPASEF mode[37] using 20 variable width isolation windows from m/z 400 to 1,350 to include the 2+/3+/4+ population in the m/z–ion mobility plane. The collision energy was ramped linearly as a function of the mobility from 59 eV at 1/K0=1.5 Vs cm^{-2} to 20 eV at 1/K0=0.7 Vs cm^{-2}. Two technical replicates per biological replicate were acquired. Protein identification was achieved using the Pulsar algorithm in Spectronaut Software version 16.0 (Biognosys) using default settings. All DIA data were searched against the UniProtKB Homo sapiens reference proteome (revision 01-2021) augmented with a set of 51 known common laboratory contaminants at default settings. For

quantitation, up to the 6 most abundant fragment ion traces per peptide, and up to the 10 most abundant peptides per protein were integrated and summed up to provide protein area values. Mass and retention time calibration as well as the corresponding extraction tolerances were dynamically determined. Both identification and quantification results were trimmed to a False Discovery Rate of 1 % using a forward-and-reverse decoy database strategy.

Statistical analysis:
Results are presented as mean ± SD (exceptions: Figure 2 g, Figure 3 e & Supplement 4, mean ± SEM) and statistical differences of experimental groups were analysed by unpaired t-test using GraphPad Prism software, where $p < 0.05$ was considered as significant. Significances were subdivided into three levels: ★ (p = 0.05 - 0.01), ★★ (p = 0.01 - 0.001), ★★★ ($p < 0.001$). The biomimetic muscle tissues for every experiment were raised on at least three different days.

Supporting Information

Supporting Information is available from the Wiley Online Library or from the authors.

Acknowledgements

The authors thank Vincent Mouly and the Myoline platform from the Institut de Myologie, Paris for generating the cells used. Additionally, we thank the Proteomics Core Facility of the University Medical Center in Göttingen for their help with mass spectrometry analysis. This work was funded by the Human Frontiers Science Program (to PMG and TB). PMG is the Canada Research Chair in Endogenous Repair. Funding to PMG is from the Natural Sciences and Engineering Research Council and Medicine by Design, a Canada First Research Excellence Program. TB was supported by the European Research Council (consolidator grant number 771201).

Conflict of Interest

The other authors declare no conflict of interest.

Supplements

Supplement 1: Representative flattened confocal stacks of healthy and DMD human bioengineered skeletal muscle tissues immunostained for dystrophin (green) and nuclei counterstained with DRAQ7 (blue).

Supplement 2: 20 Hz tetanus contraction of a Healthy1167 bioengineered skeletal muscle tissue two weeks after differentiation.

Supplement 3: Post deflection upon a 20 Hz tetanus contraction of a Healthy1167 bioengineered skeletal muscle tissue two weeks after differentiation.

Supplement 4: Correlation between the contractile force upon a 20 Hz electrical stimulation and the myotube diameter of healthy and DMD human bioengineered muscle tissues.

References

[1] M. E. Afshar, H. Y. Abraha, M. A. Bakooshli, S. Davoudi, N. Thavandiran, K. Tung, H. Ahn, H. J. Ginsberg, P. W. Zandstra, and P. M. Gilbert. A 96-well culture platform enables longitudinal analyses of engineered human skeletal muscle microtissue strength. 10(1):6918.

[2] M. Afshar Bakooshli, E. S. Lippmann, B. Mulcahy, N. Iyer, C. T. Nguyen, K. Tung, B. A. Stewart, H. van den Dorpel, T. Fuehrmann, M. Shoichet, A. Bigot, E. Pegoraro, H. Ahn, H. Ginsberg, M. Zhen, R. S. Ashton, and P. M. Gilbert. A 3d culture model of innervated human skeletal muscle enables studies of the adult neuromuscular junction. 8.

[3] D. G. Allen and N. P. Whitehead. Duchenne muscular dystrophy–what causes the increased membrane permeability in skeletal muscle? 43(3):290–294.

[4] D. G. Allen, N. P. Whitehead, and S. C. Froehner. Absence of dystrophin disrupts skeletal muscle signaling: Roles of ca2+, reactive oxygen species, and nitric oxide in the development of muscular dystrophy. 96(1):253–305.

[5] K. Arahata and A. G. Engel. Monoclonal antibody analysis of mononuclear cells in myopathies. v: Identification and quantitation of t8+ cytotoxic and t8+ suppressor cells. 23(5):493–499.

[6] I. Atanassov and H. Urlaub. Increased proteome coverage by combining PAGE and peptide isoelectric focusing: comparative study of gel-based separation approaches. 13(20):2947–2955.

[7] D. J. Blake, A. Weir, S. E. Newey, and K. E. Davies. Function and genetics of dystrophin and dystrophin-related proteins in muscle. 82(2):291–329.

[8] M. Brandt, V. Gerke, and T. Betz. Human endothelial cells display a rapid tensional stress increase in response to tumor necrosis factor-. 17(6):e0270197.

[9] J. E. Brenman, D. S. Chao, H. Xia, K. Aldape, and D. S. Bredt. Nitric oxide

synthase complexed with dystrophin and absent from skeletal muscle sarcolemma in duchenne muscular dystrophy. 82(5):743–752.

[10] M. Buckingham. Skeletal muscle formation in vertebrates. 11(4):440–448.

[11] K. Bushby, R. Finkel, D. J. Birnkrant, L. E. Case, P. R. Clemens, L. Cripe, A. Kaul, K. Kinnett, C. McDonald, S. Pandya, J. Poysky, F. Shapiro, J. Tomezsko, C. Constantin, and DMD Care Considerations Working Group. Diagnosis and management of duchenne muscular dystrophy, part 1: diagnosis, and pharmacological and psychosocial management. 9(1):77–93.

[12] J. P. Butler, I. M. Tolić-Nørrelykke, B. Fabry, and J. J. Fredberg. Traction fields, moments, and strain energy that cells exert on their surroundings. 282(3):C595–605.

[13] K. P. Campbell and S. D. Kahl. Association of dystrophin and an integral membrane glycoprotein. 338(6212):259–262.

[14] O. Campàs, T. Mammoto, S. Hasso, R. A. Sperling, D. O'Connell, A. G. Bischof, R. Maas, D. A. Weitz, L. Mahadevan, and D. E. Ingber. Quantifying cell-generated mechanical forces within living embryonic tissues. 11(2):183–189.

[15] S. Crisafulli, J. Sultana, A. Fontana, F. Salvo, S. Messina, and G. Trifirò. Global epidemiology of duchenne muscular dystrophy: an updated systematic review and meta-analysis. 15(1):141.

[16] N. A. Dumont, Y. X. Wang, J. von Maltzahn, A. Pasut, C. F. Bentzinger, C. E. Brun, and M. A. Rudnicki. Dystrophin expression in muscle stem cells regulates their polarity and asymmetric division. 21(12):1455–1463.

[17] M. Ebrahimi, H. Lad, A. Fusto, Y. Tiper, A. Datye, C. T. Nguyen, E. Jacques, L. A. Moyle, T. Nguyen, B. Musgrave, C. Chávez-Madero, A. Bigot, C. Chen, S. Turner, B. A. Stewart, E. Pegoraro, L. Vitiello, and P. M. Gilbert. De

novo revertant fiber formation and therapy testing in a 3d culture model of duchenne muscular dystrophy skeletal muscle. page S1742706121003305.

[18] Q. Q. Gao and E. M. McNally. The dystrophin complex: Structure, function, and implications for therapy. 5(3):1223–1239.

[19] R. W. Grange, E. Isotani, K. S. Lau, K. E. Kamm, P. L. Huang, and J. T. Stull. Nitric oxide contributes to vascular smooth muscle relaxation in contracting fast-twitch muscles. 5(1):35–44.

[20] S. Guiraud, A. Aartsma-Rus, N. M. Vieira, K. E. Davies, G.-J. B. van Ommen, and L. M. Kunkel. The pathogenesis and therapy of muscular dystrophies. 16:281–308.

[21] C.-P. Heisenberg and Y. Bellaïche. Forces in tissue morphogenesis and patterning. 153(5):948–962.

[22] A. D. Hofemeier, T. Limon, T. M. Muenker, B. Wallmeyer, A. Jurado, M. E. Afshar, M. Ebrahimi, R. Tsukanov, N. Oleksiievets, J. Enderlein, P. M. Gilbert, and T. Betz. Global and local tension measurements in biomimetic skeletal muscle tissues reveals early mechanical homeostasis. 10.

[23] T. Kasai, K. Abeyama, T. Hashiguchi, H. Fukunaga, M. Osame, and K. Maruyama. Decreased total nitric oxide production in patients with duchenne muscular dystrophy. 11(4):534–537.

[24] S. Klein, M. Staring, K. Murphy, M. A. Viergever, and J. P. W. Pluim. elastix: a toolbox for intensity-based medical image registration. 29(1):196–205.

[25] M. Koenig, E. Hoffman, C. Bertelson, A. Monaco, C. Feener, and L. Kunkel. Complete cloning of the duchenne muscular dystrophy (DMD) cDNA and preliminary genomic organization of the DMD gene in normal and affected individuals. 50(3):509–517.

[26] L. Lacourpaille, F. Hug, A. Guével, Y. Péréon, A. Magot, J.-Y. Hogrel, and

A. Nordez. Non-invasive assessment of muscle stiffness in patients with duchenne muscular dystrophy. 51(2):284–286.

[27] F. Lauretani, C. R. Russo, S. Bandinelli, B. Bartali, C. Cavazzini, A. Di Iorio, A. M. Corsi, T. Rantanen, J. M. Guralnik, and L. Ferrucci. Age-associated changes in skeletal muscles and their effect on mobility: an operational diagnosis of sarcopenia. 95(5):1851–1860.

[28] S. Le, M. Yu, L. Hovan, Z. Zhao, J. Ervasti, and J. Yan. Dystrophin as a molecular shock absorber. 12(12):12140–12148.

[29] B. Li, M. Lin, Y. Tang, B. Wang, and J. H.-C. Wang. A novel functional assessment of the differentiation of micropatterned muscle cells. 41(16):3349–3353.

[30] C. Long, H. Li, M. Tiburcy, C. Rodriguez-Caycedo, V. Kyrychenko, H. Zhou, Y. Zhang, Y.-L. Min, J. M. Shelton, P. P. A. Mammen, N. Y. Liaw, W.-H. Zimmermann, R. Bassel-Duby, J. W. Schneider, and E. N. Olson. Correction of diverse muscular dystrophy mutations in human engineered heart muscle by single-site genome editing. 4(1):eaap9004.

[31] L. Madden, M. Juhas, W. E. Kraus, G. A. Truskey, and N. Bursac. Bioengineered human myobundles mimic clinical responses of skeletal muscle to drugs. 4:e04885.

[32] S. M. Maffioletti, S. Sarcar, A. B. H. Henderson, I. Mannhardt, L. Pinton, L. A. Moyle, H. Steele-Stallard, O. Cappellari, K. E. Wells, G. Ferrari, J. S. Mitchell, G. E. Tyzack, V. N. Kotiadis, M. Khedr, M. Ragazzi, W. Wang, M. R. Duchen, R. Patani, P. S. Zammit, D. J. Wells, T. Eschenhagen, and F. S. Tedesco. Three-dimensional human iPSC-derived artificial skeletal muscles model muscular dystrophies and enable multilineage tissue engineering. 23(3):899–908.

[33] A. Magid and D. J. Law. Myofibrils bear most of the resting tension in frog skeletal muscle. 230(4731):1280–1282.

[34] K. Mamchaoui, C. Trollet, A. Bigot, E. Negroni, S. Chaouch, A. Wolff, P. K. Kandalla, S. Marie, J. Di Santo, J. L. St Guily, F. Muntoni, J. Kim, S. Philippi, S. Spuler, N. Levy, S. C. Blumen, T. Voit, W. E. Wright, A. Aamiri, G. Butler-Browne, and V. Mouly. Immortalized pathological human myoblasts: towards a universal tool for the study of neuromuscular disorders. 1:34.

[35] K. Maruyama. Connectin, an elastic protein from myofibrils. 80(2):405–407.

[36] E. Matthews, R. Brassington, T. Kuntzer, F. Jichi, and A. Y. Manzur. Corticosteroids for the treatment of duchenne muscular dystrophy. (5):CD003725.

[37] F. Meier, A.-D. Brunner, M. Frank, A. Ha, I. Bludau, E. Voytik, S. Kaspar-Schoenefeld, M. Lubeck, O. Raether, N. Bache, R. Aebersold, B. C. Collins, H. L. Röst, and M. Mann. diaPASEF: parallel accumulation-serial fragmentation combined with data-independent acquisition. 17(12):1229–1236.

[38] T. Muenker. Electrical stimulation. https://github.com/Tillmuen09/.

[39] T. Muenker. Post deflection analysis. https://github.com/Tillmuen09/.

[40] T. Muenker. Post distance analysis. https://github.com/Tillmuen09/.

[41] G. Mutungi, J. Trinick, and K. W. Ranatunga. Resting tension characteristics in differentiating intact rat fast- and slow-twitch muscle fibers. 95(6):2241–2247.

[42] C. T. Nguyen, M. Ebrahimi, P. M. Gilbert, and B. A. Stewart. Electrophysiological analysis of healthy and dystrophic 3-d bioengineered skeletal muscle tissues. 321(4):C749–C759.

[43] M. Periasamy, S. K. Maurya, S. K. Sahoo, S. Singh, S. K. Sahoo, F. C. G. Reis, and N. C. Bal. Role of SERCA pump in muscle thermogenesis and metabolism. 7(3):879–890.

[44] D. Piga, S. Salani, F. Magri, R. Brusa, E. Mauri, G. P. Comi, N. Bresolin, and S. Corti. Human induced pluripotent stem cell models for the study and treatment of duchenne and becker muscular dystrophies. 12:1756286419833478.

[45] J. Rahnert, X. Fan, N. Case, T. C. Murphy, F. Grassi, B. Sen, and J. Rubin. The role of nitric oxide in the mechanical repression of RANKL in bone stromal cells. 43(1):48–54.

[46] M. P. Ramirez, M. J. Anderson, L. J. Sundby, A. R. Hagerty, S. J. Wenthe, J. M. Ervasti, and W. R. Gordon. Dystrophin modulates focal adhesion tension and YAP-mediated mechanotransduction.

[47] M. Rausch, D. Böhringer, M. Steinmann, D. W. Schubert, S. Schrüfer, C. Mark, and B. Fabry. Measurement of skeletal muscle fiber contractility with high-speed traction microscopy. 118(3):657–666.

[48] M. Rief, J. Pascual, M. Saraste, and H. E. Gaub. Single molecule force spectroscopy of spectrin repeats: low unfolding forces in helix bundles. 286(2):553–561.

[49] J. Schindelin, I. Arganda-Carreras, E. Frise, V. Kaynig, M. Longair, T. Pietzsch, S. Preibisch, C. Rueden, S. Saalfeld, B. Schmid, J.-Y. Tinevez, D. J. White, V. Hartenstein, K. Eliceiri, P. Tomancak, and A. Cardona. Fiji: an open-source platform for biological-image analysis. 9(7):676–682.

[50] H. Schürmann, F. Abbasi, A. Russo, A. D. Hofemeier, M. Brandt, J. Roth, T. Vogl, and T. Betz. Analysis of monocyte cell tractions in 2.5d reveals mesoscale mechanics of podosomes during substrate-indenting cell protrusion. 135(10):jcs259042.

[51] M. Shahriyari, M. R. Islam, S. M. Sakib, M. Rinn, A. Rika, D. Krüger, L. Kaurani, V. Gisa, M. Winterhoff, H. Anandakumar, O. Shomroni, M. Schmidt, G. Salinas, A. Unger, W. A. Linke, J. Zschüntzsch, J. Schmidt, R. Bassel-Duby, E. N. Olson, A. Fischer, W. Zimmermann, and M. Tiburcy.

Engineered skeletal muscle recapitulates human muscle development, regeneration and dystrophy. page jcsm.13094.

[52] D. Shamonin. Fast parallel image registration on CPU and GPU for diagnostic classification of alzheimer's disease. 7.

[53] H. Shams, J. Golji, and M. R. K. Mofrad. A molecular trajectory of -actinin activation. 103(10):2050–2059.

[54] R. Spörle. Epaxial-adaxial-hypaxial regionalisation of the vertebrate somite: evidence for a somitic organiser and a mirror-image duplication. 211(4):198–217.

[55] M. Spörrer, D. Kah, R. C. Gerum, B. Reischl, D. Huraskin, C. A. Dessalles, W. Schneider, W. H. Goldmann, H. Herrmann, I. Thievessen, C. S. Clemen, O. Friedrich, S. Hashemolhosseini, R. Schröder, and B. Fabry. The desmin mutation r349p increases contractility and fragility of stem cell-generated muscle micro-tissues. 48(3).

[56] J. G. Tidball, E. Lavergne, K. S. Lau, M. J. Spencer, J. T. Stull, and M. Wehling. Mechanical loading regulates NOS expression and activity in developing and adult skeletal muscle. 275(1):C260–266.

[57] L. Viollet, P. T. Thrush, K. M. Flanigan, J. R. Mendell, and H. D. Allen. Effects of angiotensin-converting enzyme inhibitors and/or beta blockers on the cardiomyopathy in duchenne muscular dystrophy. 110(1):98–102.

[58] M. Walker, P. Rizzuto, M. Godin, and A. E. Pelling. Structural and mechanical remodeling of the cytoskeleton maintains tensional homeostasis in 3d microtissues under acute dynamic stretch. 10(1):7696.

[59] N. Wein, A. Vulin, M. S. Falzarano, C. A.-K. Szigyarto, B. Maiti, A. Findlay, K. N. Heller, M. Uhlén, B. Bakthavachalu, S. Messina, G. Vita, C. Passarelli, S. Brioschi, M. Bovolenta, M. Neri, F. Gualandi, S. D. Wilton, L. R. Rodino-Klapac, L. Yang, D. M. Dunn, D. R. Schoenberg, R. B. Weiss, M. T. Howard,

A. Ferlini, and K. M. Flanigan. Translation from a DMD exon 5 IRES results in a functional dystrophin isoform that attenuates dystrophinopathy in humans and mice. 20(9):992–1000.

[60] R. J. Willcocks, S. C. Forbes, G. A. Walter, L. Sweeney, L. R. Rodino-Klapac, J. R. Mendell, and K. Vandenborne. Assessment of rAAVrh.74.MHCK7.micro-dystrophin gene therapy using magnetic resonance imaging in children with duchenne muscular dystrophy. 4(1):e2031851.

[61] R. Willmann, S. Possekel, J. Dubach-Powell, T. Meier, and M. A. Ruegg. Mammalian animal models for duchenne muscular dystrophy. 19(4):241–249.

[62] K. Wilson, C. Faelan, J. C. Patterson-Kane, D. G. Rudmann, S. A. Moore, D. Frank, J. Charleston, J. Tinsley, G. D. Young, and A. J. Milici. Duchenne and becker muscular dystrophies: A review of animal models, clinical end points, and biomarker quantification. 45(7):961–976.